

# Evolution of clustering in cosmological models with time-varying dark energy

Tomoaki Ishiyama\*

*Digital Transformation Enhancement Council, Chiba University,  
1-33, Yayoi-cho, Inage-ku, Chiba, 263-8522, Japan*

Francisco Prada

*Instituto de Astrofísica de Andalucía (CSIC), Glorieta de la Astronomía, E-18080 Granada, Spain*

Anatoly A. Klypin

*Astronomy Department, New Mexico State University, Las Cruces, NM, USA and  
Department of Astronomy, University of Virginia, Charlottesville, VA, USA*

(Dated: March 28, 2025)

Observations favor cosmological models with a time-varying dark energy component. But how does dynamical dark energy (DDE) influence the growth of structure in an expanding Universe? We investigate this question using high-resolution  $N$ -body simulations based on a DDE cosmology constrained by first-year DESI data (DESIY1+DDE), characterized by a 4% lower Hubble constant ( $H_0$ ) and 10% higher matter density ( $\Omega_0$ ) than the Planck-2018  $\Lambda$ CDM model. We examine the impact on the matter power spectrum, halo abundances, clustering, and Baryonic Acoustic Oscillations (BAO). We find that DESIY1+DDE exhibits a 10% excess in power at small scales and a 15% suppression at large scales, driven primarily by its higher  $\Omega_0$ . This trend is reflected in the halo mass function: DESIY1+DDE predicts up to 70% more massive halos at  $z = 2$  and a 40% excess at  $z = 0.3$ . Clustering analysis reveals a 3.71% shift of the BAO peak towards smaller scales in DESIY1+DDE, consistent with its reduced sound horizon compared to Planck18. Measurements of the BAO dilation parameter  $\alpha$ , using halo samples with DESI-like tracer number densities across  $0 < z < 1.5$ , agree with the expected DESIY1+DDE-to-Planck18 sound horizon ratio. After accounting for cosmology-dependent distances, the simulation-based observational dilation parameter closely matches DESI Y1 data. We find that the impact of DDE is severely limited by current observational constraints, which strongly favor cosmological models – whether including DDE or not – with a tightly constrained parameter  $\Omega_0 h^2 \approx 0.143$ , within 1-2% uncertainty. Indeed, our results demonstrate that variations in cosmological parameters, particularly  $\Omega_0$ , have a greater influence on structure formation than the DDE component alone.

## I. INTRODUCTION

Measurements of the Baryon Acoustic Oscillations (BAO) feature in the clustering of galaxies from the first- and third-year data of the Dark Energy Spectroscopic Instrument (DESI Y1 and Y3 [1, 2]), combined with the Cosmic Microwave Background (CMB) anisotropies from the Planck satellite (Planck18 [3]), indicate a preference for a time-varying Dynamic Dark Energy (DDE) equation of state, with a deviation from  $\Lambda$ CDM at the  $\sim 3.1\sigma$  level. Including type Ia supernovae (SN Ia) data alongside with DESIY1 BAO and CMB measurements further increases the statistical significance of DDE signal, reaching between  $\sim 2.8\sigma$  and  $\sim 4.2\sigma$ , depending on the specific SN Ia dataset used (see [2]).

Several DDE models have been proposed in the literature [4–8]. Among them, the Chevallier-Polarski-Linder (CPL) parametrization [5, 6] is one of the most widely used formulations of a time-varying dark energy equation of state, and is frequently adopted in the analysis of observational data. In this model, the dark energy equation

of state parameter  $w$  evolves with the scale factor  $a$  as:

$$w(a) = w_0 + w_a(1 - a), \quad (1)$$

where  $w_0$  and  $w_a$  are free parameters.

Notably, the values of the matter density  $\Omega_0$  and Hubble constant ( $H_0 = 100 h$  km/sec/Mpc), derived when including DESI data, differ significantly from those inferred from Planck-only constraints. The DESIY1 data suggests a  $\sim 10\%$  higher matter density and a  $\sim 4\%$  lower Hubble constant, with best-fit DDE parameters  $w_0 = -0.45$  and  $w_a = -1.79$ . The resulting cosmological parameters, summarized in Table I, define the DESIY1+DDE cosmology used throughout this work. For comparison, we also consider the baseline Planck18 model based on Planck-2018 results [3], as well as a hybrid model Planck18+DDE that adopts Planck-2018 values for standard cosmological parameters but uses the  $w_0$  and  $w_a$  parameters from DESIY1+DDE. Table I also gives the corresponding values of the baryon drag epoch  $z_d$  and the comoving sound horizon scale  $r_d$ . These differences among the three models can have a substantial impact on various large-scale structure (LSS) observables, including the power spectrum, the abundance of galaxies (dark matter halos), and their clustering properties.

Cosmological simulations are powerful tools to studying non-linear structure growth and for accurately es-

---

\* e-mail:ishiyama@chiba-u.jp

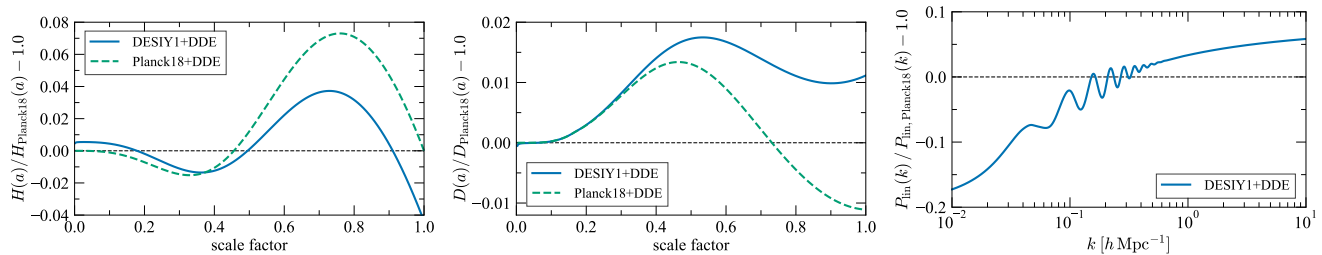


FIG. 1. Evolution of the Hubble parameter (left), linear growth factor (middle), and the linear matter power spectrum (right) for the cosmological models indicated in the labels, shown relative to the Planck18 model.

timating key statistical measures. A number of studies have employed  $N$ -body simulations to explore DDE models [e.g., 9–13]. However, the volumes of recent galaxy surveys are extremely large, leading to relatively small statistical uncertainties. To match this precision, high-resolution cosmological simulations based on DDE must cover similarly large volumes. Such large-volume simulations are not that common for DDE, in sharp contrast to the extensive suite of concordance  $\Lambda$ CDM simulations [e.g., 14–18].

Beltz-Mohrmann et al. [13] performed two large  $N$ -body simulations of DDE models, each with a box size of  $1 h^{-1}$ Gpc. Their results on the nonlinear dark matter power spectra and halo mass functions are qualitatively consistent with our findings. In this regard, their results and ours are complimentary. However, Beltz-Mohrmann et al. [13] did not study the clustering of dark matter halos, nor did they analyze fluctuations in the BAO domain - an essential aspect for interpreting DESI observations and one of the main focuses of our work. Such an analysis requires either a very large computational box or many realizations to overcome the significant cosmic variance at BAO scales. Our simulations enable this analysis, as their total volume is eight times larger than that of Beltz-Mohrmann et al. [13].

In this work, we perform large cosmological  $N$ -body simulations using cosmological parameters that include DDE parameters constrained by DESIY1 data, and investigate the impact of DDE on various LSS statistics. This paper is organized as follows. Dynamical Dark Energy models are introduced in Sec. II. In Sec. III, we describe the cosmological simulations in detail. Results are presented in Sec. IV, followed by a discussion in Sec. V. Our main findings are summarized in Sec. VI.

## II. DYNAMICAL DARK ENERGY COSMOLOGY

The evolution of the Hubble constant in DDE model with CPL parametrization is given by

$$\left[ \frac{H(a)}{H_0} \right]^2 = \frac{\Omega_0}{a^3} + \frac{\lambda_0}{a^{3(1+w_a+w_0)}} \exp(-3w_a(1-a)). \quad (2)$$

TABLE I. Estimates of cosmological parameters from the Planck (Planck18) [3] and DESI (DESIY1+DDE) [1] experiments are shown. Here,  $z_d$  denotes the baryon drag epoch, and  $r_d$  is the comoving sound horizon scale. In addition to these two models, we also consider a third model in this paper, denoted as (Planck18+DDE), which adopts the same cosmological parameter as Planck18, but includes the effects of dynamical dark energy.

Parameter	Planck18	Planck18+DDE	DESIY1+DDE
$\Omega_0$	0.3111	0.3111	0.3440
$h$	0.6766	0.6766	0.6470
$w_0$	-1.0	-0.45	-0.45
$w_a$	0.0	-1.79	-1.79
$z_d$	1060.02	1060.02	1055.70
$r_d$ [ $h^{-1}$ Mpc]	99.61	99.61	96.05

The left and middle panels in Figure 1 show the evolution of the Hubble parameter and linear growth factor for the DESIY1+DDE and Planck18+DDE models, relative to those of the Planck18 model. Both quantities deviate from the Planck18 model by at most  $\sim 4\%$ . While these differences are relatively small, they are potentially measurable. Most of the deviations occur at low redshifts ( $z < 1$ , or equivalently, scale factor  $a > 0.5$ ), whereas at higher redshifts the differences become negligible.

The main cosmological parameters of the three models studied in this work are listed in Table I. All other parameters are identical across the models:  $\Omega_b = 0.048975$ ,  $n_s = 0.9665$ , and  $\sigma_8 = 0.8102$ . It is important to note that power spectrum of density fluctuations depends critically on a combination  $\Omega_0 h^2$ , which determines the location of the peak in the power spectrum. The trio of parameters  $\Omega_0 h^2$ ,  $n_s$  and  $\sigma_8$  nearly - but not entirely - fixes the shape and amplitude of the linear perturbation spectrum. In all three models considered here, these three parameters are the same. What differs among the models is the baryons fraction  $\Omega_b/\Omega_0$ , which influences the power spectrum at the  $\sim 10\%$  level and is primarily responsible for the differences in the BAO features observed in the spectrum.

The right panel of Figure 1 shows the differences in the linear power spectra between the DESIY1+DDE and Planck18 models. The Planck18+DDE model shares the

same linear power spectrum as Planck18, since they have identical early-Universe parameters. In contrast, the DESIY1+DDE model exhibits notable deviations: an increase in power of  $\sim 5\%$  at small scales  $k > 1 h \text{ Mpc}^{-1}$  and a decline of  $\sim 20\%$  at large (Gpc) scales  $k < 0.01 h \text{ Mpc}^{-1}$ . These changes in the shape of the power spectrum are an indirect consequence of adopting a dynamical dark energy model. While DDE does not directly impact the physics of the early Universe that sets the linear power spectrum of fluctuations, adopting DDE parameters leads to different best-fit values of  $H_0$ ,  $\Omega_0$  and  $\Omega_{\text{baryon}}$  that remain consistent with observational constraints. It is these altered parameters that drive the significant modifications observed in the power spectrum. The increase in power spectrum at large wavenumbers significantly impacts the evolution of the halo mass function and, consequently, galaxy formation. Due to the higher amplitude of fluctuations, halos collapse earlier, leading to an overall increase in their abundance. This shift in amplitude affects massive halos more strongly than low-mass halos. In summary, the DDE models DESIY1+DDE and Planck18+DDE are expected to produce a higher number of halos (and hence galaxies) compared to the Planck18 model.

### III. COSMOLOGICAL $N$ -BODY SIMULATIONS

We perform three cosmological  $N$ -body simulations, each with a box size of  $L = 2000 h^{-1} \text{ Mpc}$  and a particle number of  $N = 4096^3$ . The particle mass resolution is  $m_p = 1.0 \times 10^{10} h^{-1} \text{ M}_\odot$  for the Planck18 and Planck18+DDE simulations, and  $m_p = 1.1 \times 10^{10} h^{-1} \text{ M}_\odot$  for the DESIY1+DDE simulation.

Initial conditions were generated using the publicly available code, MONOFONIC<sup>1</sup> [19, 20], using third-order Lagrangian perturbation theory. All three simulations share the same initial phase and starting redshift ( $z_{\text{ini}} = 24$ ), allowing us to ignore the impact of cosmic variance. The matter transfer functions were computed using the Python version of CAMB<sup>2</sup>[21].

We follow the non-linear gravitational evolution of dark matter using the massively parallel TreePM code GREEM<sup>3</sup> [22–24], run on the Fugaku supercomputer at the RIKEN Center for Computational Science. To incorporate the effects of dynamical dark energy, we implemented Eq (2) into the GREEM code. The plummer gravitational softening length was set to  $\varepsilon = 8.0 h^{-1} \text{ kpc}$ . We used the PHANTOM-GRAPE<sup>4</sup> code [25–28] to accelerate the pairwise gravity force calculation. Halos and subhalo identification was performed using MPI-ROCKSTAR<sup>5</sup> [29], a hybrid MPI and OpenMP massively

parallel code, which is an extension of the original ROCKSTAR phase space (sub)halo finder<sup>6</sup> [30]. The resulting HDF5 halo catalogs are publicly available on the Skies & Universes site at <https://skun.iaa.csic.es/SUsimulations/DDE/>.

## IV. RESULTS

We compare the basic clustering properties of dark matter and halos across the three simulation models, focusing on the matter power spectrum, halo mass function, and the redshift-space two-point correlation functions and power spectra of halo samples. These quantities are analyzed at redshifts  $z = 2.03, 1.54, 0.78, 0.30$ , and 0, chosen to match those of the DESI samples of luminous tracers [1].

### A. Power spectra

Figure 2 shows the matter power spectra of DESIY1+DDE and Planck18+DDE models relative to the Planck18 simulation for the range  $0.1 < k < 10 h \text{ Mpc}^{-1}$ . At redshifts  $z \gtrsim 1.54$ , the power spectrum of the Planck18+DDE model is a few percent higher than that of Planck18. This difference gradually decreases with redshifts and becomes negligible (within 1%) by  $z = 0.3$ . This trend is explained by the evolution of the linear growth factor, shown in Figure 1. The growth factor in the Planck18+DDE model relative to Planck18 increases with time, peaking around  $z \sim 1$ , and then gradually decreases toward  $z = 0$ . A larger (smaller) growth factor enhances (suppresses) the power spectrum. However, since the maximum difference in the growth factor is only about 1%, the resulting enhancement in power remains at the level of just a few percent.

Comparison of the DESIY1+DDE and Planck18 results reveals a more complex situation, primarily due to the differences in the initial matter power spectra, as shown in Figure 1. The BAO pattern around  $k \gtrsim 0.1 h \text{ Mpc}^{-1}$  is visible in the relative power spectrum because the sound horizon scale is slightly smaller in the DESIY1+DDE model compared to Planck18 (see Table I). This pattern persists in the relative power at all redshift. For  $k \gtrsim 0.2 h \text{ Mpc}^{-1}$ , the initial power in DESIY1+DDE is consistently higher than in Planck18 by up to  $\sim 10\%$ . Additionally, the growth factor is systematically larger in DESIY1+DDE due to its  $\sim 10\%$  higher value of  $\Omega_0$ , which helps counteract the suppressive effect of DDE at  $z \gtrsim 0.5$ . As a result, the relative power difference with respect to Planck18 is larger in DESIY1+DDE than in Planck18+DDE, except at very

<sup>1</sup> <https://bitbucket.org/ohahn/monofonic/>

<sup>2</sup> <https://camb.info/>

<sup>3</sup> <http://hpc.imit.chiba-u.jp/~ishiytm/greem/>

<sup>4</sup> <https://bitbucket.org/kohji/phantom-grape/src>

<sup>5</sup> <https://github.com/Tomoaki-Ishiyama mpi-rockstar/>

<sup>6</sup> <https://bitbucket.org/gfcstanford/rockstar/>

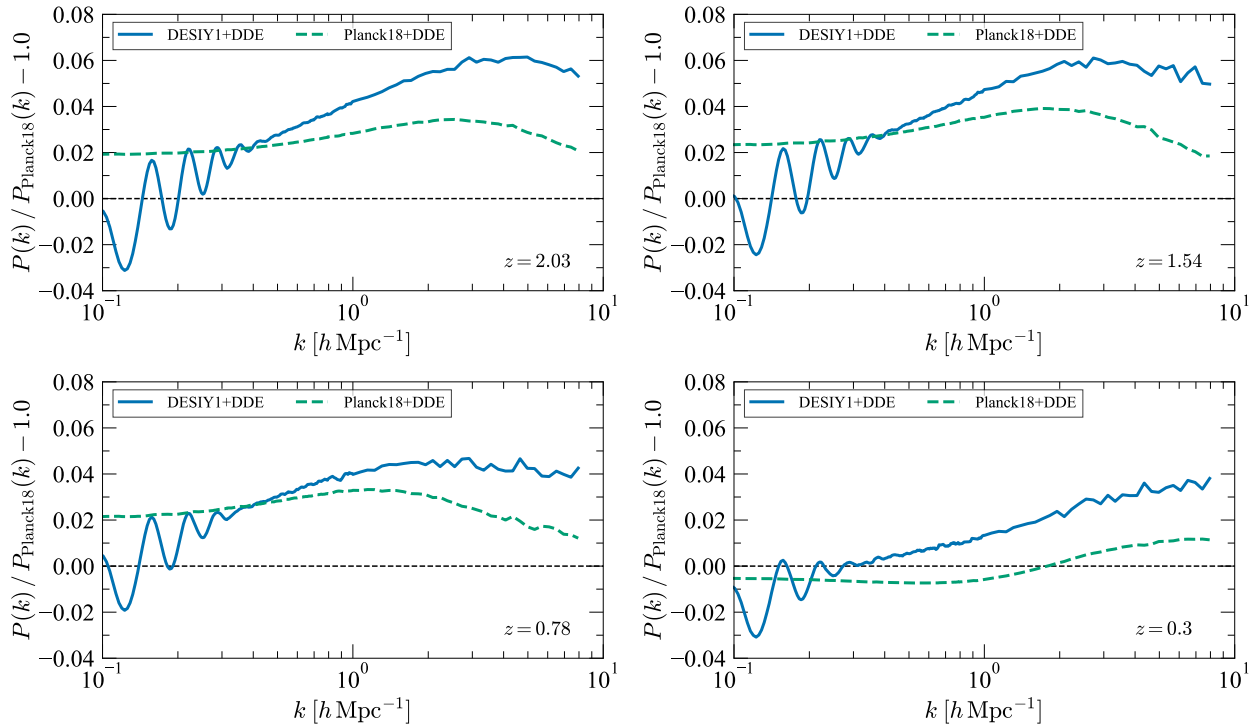


FIG. 2. Matter power spectra of the DESIY1+DDE and Planck18+DDE models relative to the Planck18 simulation at  $z = 2.03, 1.54, 0.78$ , and  $0.30$ . The relative differences decrease toward lower redshifts, although the power spectra differ by less than 10% at all redshifts. The difference in cosmological parameters between the Planck18 and DESIY1-based models has a more significant impact on the power spectrum than the effect of dynamical dark energy.

small  $k$ , where the initial power in DESIY1+DDE is approximately  $\sim 15\%$  lower than in Planck18. Overall, the differences in cosmological parameters - particularly  $\Omega_0$  - have a more significant impact on the matter power spectrum than the DDE effect alone.

### B. Halo mass function

Figure 3 shows the halo mass functions of the DESIY1+DDE and Planck18+DDE simulations relative to the Planck18 simulation. We only show results for halos more massive than  $4.0 \times 10^{11} h^{-1} M_\odot$ , corresponding to  $\sim 40$  particles per halo. At all redshift, the DESIY1+DDE model predicts a higher abundance of massive halos compared to Planck18, with differences reaching up to  $\sim 70\%$ . As discussed in Sec.II, this is a consequence of the altered shape of the linear power spectrum: the DESIY1+DDE model features a higher amplitude of fluctuations on galactic and cluster scales, which leads to earlier and more efficient formation of halos. The abundance of rare, high-mass halos is particularly sensitive to changes in amplitude, which explains why the excess number of halos in DESIY1+DDE increases with halo mass.

There is a slight excess in the number of halos in the Planck18+DDE model, but it is dramatically

smaller than in the DESIY1+DDE model. Note that Planck18+DDE and Planck18 models share the same cosmological parameters, differing only in the nature of dark energy. Therefore, the difference between these two models arises solely from the variation in the growth rate of fluctuations, not from differences in the initial power spectrum (see the middle panel in Figure 1). Since the growth rates differ by only  $\sim 1\%$ , the resulting change in halo abundance is modest and vanishes by redshift  $z = 0.3$ .

The evolution of the halo mass function exhibits a similar trend to that seen in the power spectra: the excess relative to Planck18 decreases towards lower redshifts for both the DESIY1+DDE and Planck18+DDE models. In the case of Planck18+DDE, the difference disappears by  $z = 0.3$ . However, the DESIY1+DDE model still predicts  $\sim 40\%$  more massive clusters at that redshift, which could serve as an additional cosmological test.

### C. Baryonic Acoustic Oscillations: Planck18 vs. DESIY1+DDE

We study the clustering of dark matter halos in redshift space on scales  $50\text{--}150 h^{-1} \text{Mpc}$ , which are relevant for measurements of the BAO feature. Real-space halo positions are displaced into the redshift space along each of the  $x$ -,  $y$ - and  $z$ -axis, and the correlation functions are

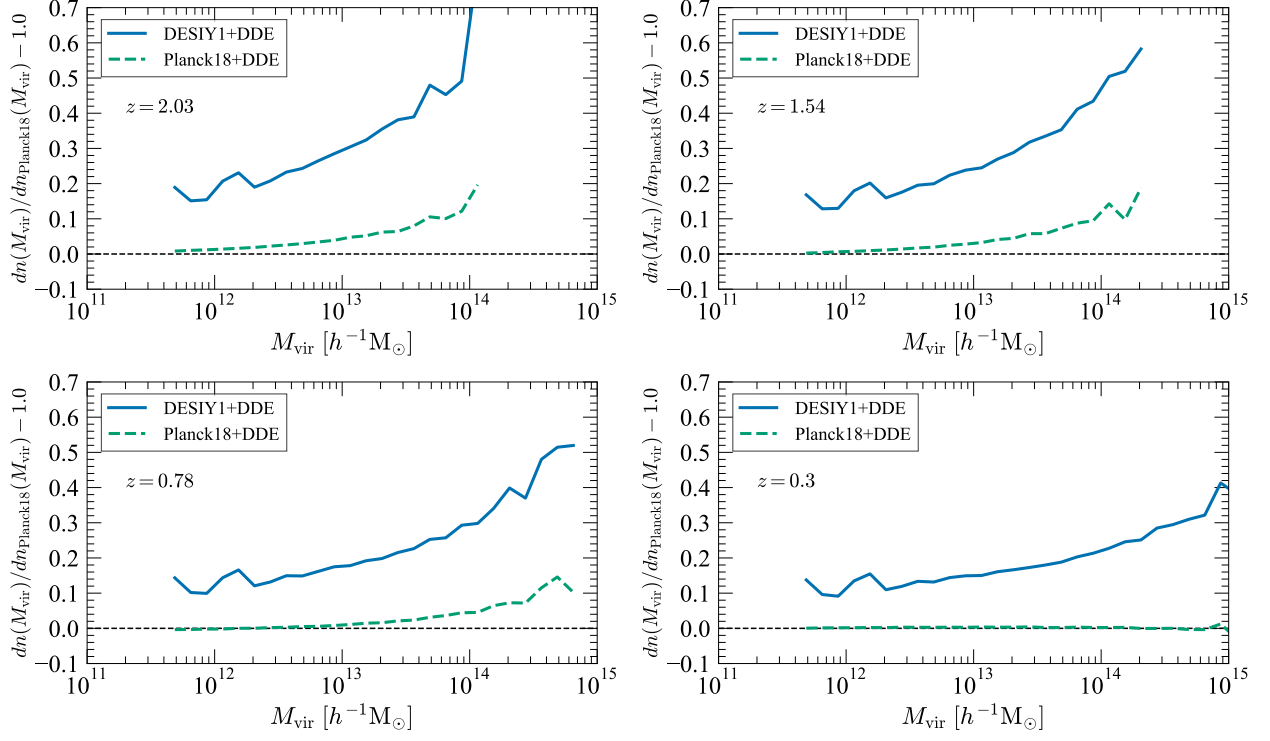


FIG. 3. Halo mass functions of the DESIY1+DDE and Planck18+DDE models relative to Planck18 simulation at  $z = 2.03, 1.54, 0.78$ , and  $0.30$ . The relative differences decrease toward lower redshift, and the effect of DDE becomes negligible by  $z = 0.3$ . The difference in cosmological parameters between the Planck18 and DESIY1-based models has a more significant impact than the effect of DDE.

calculated using the CORRFUNC<sup>7</sup> [31, 32] code with the Landy-Szalay estimator [33]. The resulting correlation functions along the three axes are averaged and analyzed.

The monopole of the redshift-space two-point correlation function,  $\xi_0(s)$ , scaled by  $s^2$ , is shown in Figure 4 as a function of the comoving separation  $s$ . The analysis includes four halo samples drawn from the three cosmological simulations, with number densities (in units of  $(h^{-1}\text{Mpc})^3$ ) set to  $1.0 \times 10^{-4}$  at  $z = 2.03$  and  $1.54$ ,  $4.0 \times 10^{-4}$  at  $z = 0.78$ , and  $3.0 \times 10^{-4}$  at  $z = 0.30$ . These  $n(z)$  values are chosen to represent the observed number densities of the DESIY1 galaxy and QSO data samples used in BAO measurements [1].

A distinct BAO peak is clearly visible at  $s \approx 100 h^{-1}\text{Mpc}$  across all samples. The position of this peak is a key cosmological observable, serving as a standard ruler for distance measurements and for inferring the expansion history of the universe [34].

At all redshifts, the BAO peak in the DESIY1+DDE model is shifted by  $\sim 4\%$  toward smaller scales (i.e., lower values of  $s$ ) compared to the Planck18 model, as expected from differences in their sound horizon scale at the drag epoch (see Table 1). In the DESIY1+DDE model, the

BAO feature appears sharper and has a slightly reduced amplitude at higher redshifts ( $z = 2.03$  and  $1.54$ ), where the clustering signal is less affected by nonlinear evolution and redshift-space distortions. In contrast, in the Planck18 model, the BAO features become more damped and broader at lower redshifts ( $z = 0.78$  and  $0.30$ ) due to stronger nonlinear effects. The two-point correlation function of the Planck18+DDE model is indistinguishable from that of the Planck18, as both share the same initial BAO pattern in the power spectrum and similar fluctuation amplitudes.

Non-linear evolution broadens the BAO features but does not alter the relative shift between the two models, which is set at the last scattering surface, as shown in Figure 5. This figure displays the deviations of each linear power spectrum from the corresponding ‘non-wiggle’ reference spectrum, derived using the fitting formula of Eisenstein and Hu [34] for  $P_{\text{nw}}(k)$ , which excludes the BAO features. The separation between the BAO peaks in the power spectrum scales with the isotropic dilation parameter  $\alpha$ , which accounts for the rescaling of wavenumbers between the two cosmologies. The relationship between the power spectra of the DESIY1+DDE and Planck18 models is given by the transformation:

$$P_{\text{DESI}}(k) = \frac{1}{\alpha^3} P_{\text{PL}}\left(\frac{k}{\alpha}\right). \quad (3)$$

<sup>7</sup> <https://github.com/manodeep/Corrfunc>

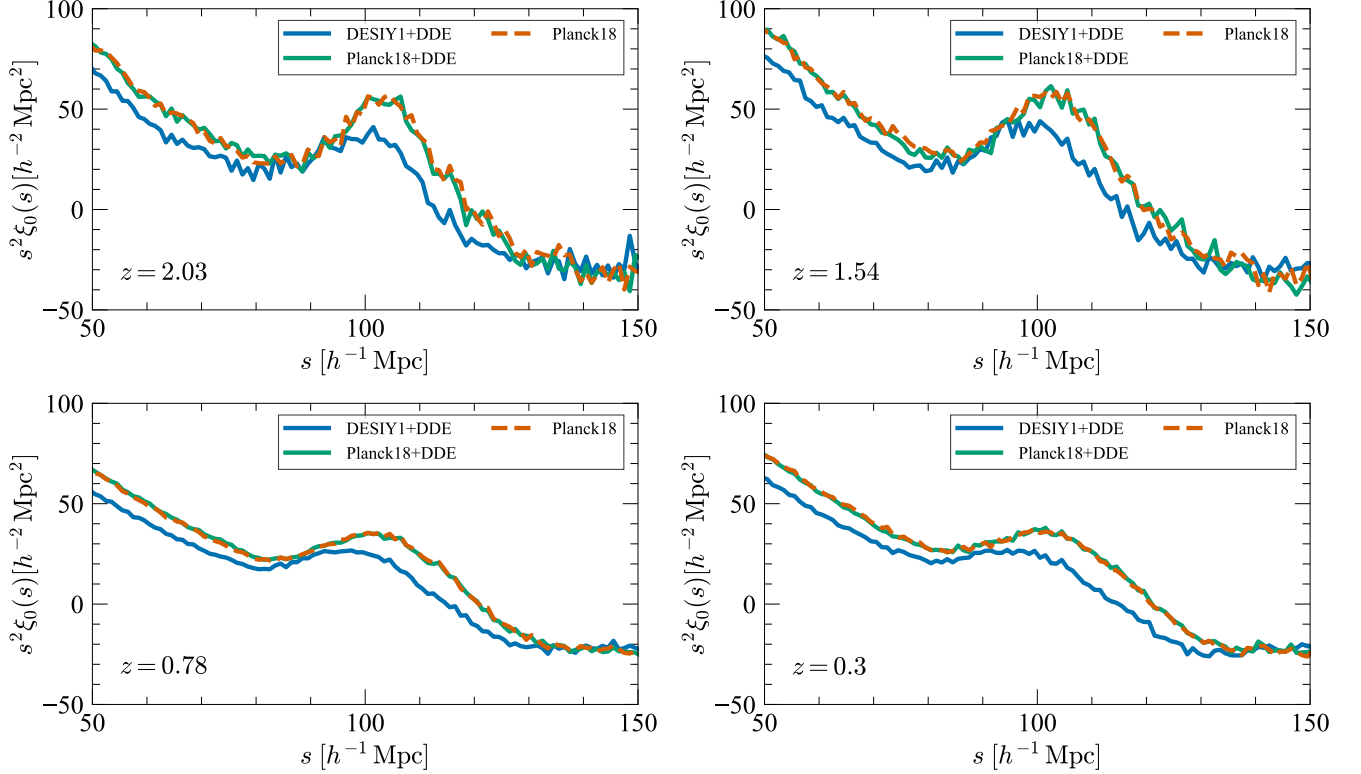


FIG. 4. Monopole of redshift-space two-point correlation function,  $\xi_0$ , scaled by  $s^2$ , as a function of comoving separation  $s$ , for all three simulations at redshifts  $z = 2.03, 1.54, 0.78$ , and  $0.30$ , as indicated in each panel. The BAO peak at  $s \sim 100 h^{-1} \text{Mpc}$  is clearly visible at all redshifts. In the DESIY1+DDE model, the peak is shifted by approximately 4% toward smaller values of  $s$  compared to the Planck18 model. This shift is expected due to differences in the sound horizon scales between the models at the drag epoch (see Table I).

The positions of the BAO peaks in  $k$ -space are systematically shifted according to  $k_{\text{DESI}} = \alpha k_{\text{PL}}$ . Thus, the parameter  $\alpha$  reflects the scaling of the sound horizon and is defined as the ratio of the sound horizon scales, in units of  $h^{-1} \text{Mpc}$ , between the two cosmologies:

$$\alpha = \frac{r_d^{\text{PL}}}{r_d^{\text{DESI}}}. \quad (4)$$

Since  $\alpha > 1$ , with  $\alpha = 1.0371$  based on the  $r_d$  values from Table 1, the BAO peak positions in the linear DESIY1+DDE power spectrum are systematically shifted towards larger wavenumbers relative to those in Planck18 as shown in Figure 5.

We measure the BAO shifts in the DESIY1+DDE simulation comoving boxes relative to those from Planck18 for the halo samples with number densities and redshifts listed in Table II. This is done by modeling the non-linear halo power spectra in redshift space, where the acoustic oscillation features of the linear Planck18 power spectrum are damped using a Gaussian function. The scale parameter of this Gaussian accounts for the broadening of the BAO features due to non-linear effects. The functional form used follows Eq. (2) from Klypin et al. [35] (see references therein). In our model, the BAO shift, quantified

by  $\alpha_{\text{sim}}$ , and the damping of the acoustic oscillations are treated as free parameters.

We then fit the power spectra  $P(k)$  over the wavenumber range  $0.05 < k < 0.3 h \text{Mpc}^{-1}$ . The resulting best-fit values of  $\alpha_{\text{sim}}$  are provided in Table II for the halo samples drawn from our Planck18 and DESIY1+DDE simulations, listed in the third and fourth columns, respectively, covering redshift from 0 to 1.5. We expect slightly larger BAO shifts in  $\alpha_{\text{sim}}$ , particularly at higher  $k$ , with deviations about 0.25% compared to the sound horizon ratio  $\alpha = 1.0371$ , due to non-linear effects [36]. This behavior is indeed observed in the DESIY1+DDE simulation results ( $\alpha_{\text{sim}}^{\text{DESI}}$ ).

To convert the BAO shifts obtained from the DESIY1+DDE comoving simulation boxes,  $\alpha_{\text{sim}}^{\text{DESI}}$ , into the isotropic dilation parameter used in DESI observations, it is necessary to account for cosmology-dependent distances and adopt a fiducial cosmology. Assuming Planck18 as the fiducial cosmology, the simulation-based observational dilation parameter  $\alpha_{\text{obs}}^{\text{DESI}}$ , is defined as,

$$\alpha_{\text{obs}} = \alpha_{\text{sim}} \frac{h^{\text{PL}}}{h^{\text{DESI}}} \frac{D_V^{\text{DESI}}(z)}{D_V^{\text{PL}}(z)}, \quad (5)$$

where  $D_V(z) = \left[ (1+z)^2 D_A(z)^2 \frac{cz}{H(z)} \right]^{1/3}$  is the volume-



TABLE II. Best-fit values of the BAO shift parameter measured from the Planck18 ( $\alpha_{\text{sim}}^{\text{PL}}$ ) and DESIY1+DDE ( $\alpha_{\text{sim}}^{\text{DESI}}$ ) simulations across different redshifts ( $z$ ) for the corresponding halo number densities ( $n$ ) in units of  $\text{Mpc}^{-3}h^3$ . The fifth column shows the ratio of the volume-averaged distance between the DESIY1+DDE and Planck18 cosmologies,  $D_V^{\text{DESI}}/D_V^{\text{PL}}$ . The sixth column presents the simulation-based observational dilation parameter,  $\alpha_{\text{obs}}^{\text{DESI}}$ , obtained by converting the comoving simulation box values  $\alpha_{\text{sim}}$  using Eq. (5). The final column lists the theoretical predictions,  $\alpha_{\text{th}}^{\text{DESI}}$ , based on the DESIY1 cosmology.

$z$	$n$	$\alpha_{\text{sim}}^{\text{PL}}$	$\alpha_{\text{sim}}^{\text{DESI}}$	$D_V^{\text{DESI}}/D_V^{\text{PL}}$	$\alpha_{\text{obs}}^{\text{DESI}}$	$\alpha_{\text{th}}^{\text{DESI}}$
1.54	$1.0 \times 10^{-4}$	$0.9957 \pm 0.0027$	$1.0374 \pm 0.0037$	0.9970	$0.9894 \pm 0.0035$	0.98871
0.78	$4.0 \times 10^{-4}$	$1.0012 \pm 0.0032$	$1.0390 \pm 0.0038$	0.9826	$0.9762 \pm 0.0036$	0.97440
0.30	$3.0 \times 10^{-4}$	$0.9994 \pm 0.0040$	$1.0395 \pm 0.0050$	0.9838	$0.9779 \pm 0.0047$	0.97565
0.00	$3.0 \times 10^{-4}$	$0.9964 \pm 0.0051$	$1.0395 \pm 0.0061$	1.0457	$1.0395 \pm 0.0061$	1.03706

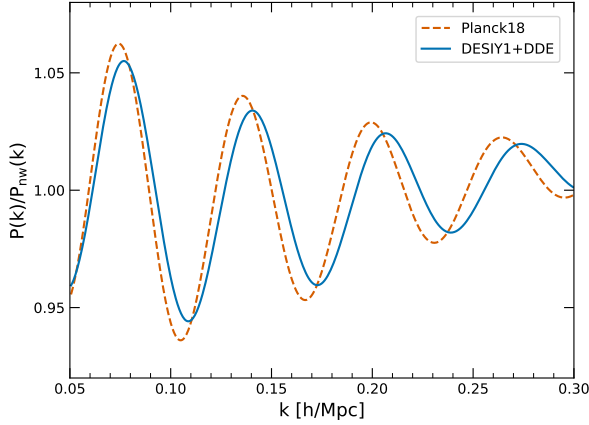


FIG. 5. Baryonic acoustic oscillations in the linear power spectrum for the DESIY1+DDE (solid curve) and Planck18 (dashed curve) cosmologies. The plot shows the deviations of each power spectrum from the corresponding “no-wiggle” reference spectrum - i.e., one without baryonic oscillations - adopted from Eisenstein and Hu [34]. Compared to Planck18, the BAO peaks in the DESIY1+DDE cosmology are systematically shifted by 3.71% toward larger wavenumbers, reflecting the difference in the sound horizon scale at the drag epoch.

averaged (dilation) distance, in units of Mpc [37]. Here,  $D_A(z)$  is the angular diameter distance (in Mpc), and  $H(z)$  is the Hubble parameter at redshift  $z$  (in  $\text{km s}^{-1} \text{Mpc}^{-1}$ ). The ratio of the dimensionless Hubble parameter between the fiducial Planck18 and DESIY1+DDE cosmologies accounts for converting the sound horizon ratio, originally expressed in  $h^{-1}\text{Mpc}$ , to physical units of Mpc. This correction ensures consistency when comparing the simulation-derived BAO shift parameter,  $\alpha_{\text{sim}}$ , with observational results. In Table II, we report the values of  $D_V^{\text{DESI}}/D_V^{\text{PL}}$  and the corresponding observational dilation parameter in the DESIY1+DDE cosmology in the fifth and sixth columns, respectively, computed using Eq. (5).

The BAO shifts obtained from our DESIY1+DDE simulation, relative to the predictions from the Planck18 cosmology (adopted as the fiducial model), are shown in Figure 6. The blue symbols represent the simula-

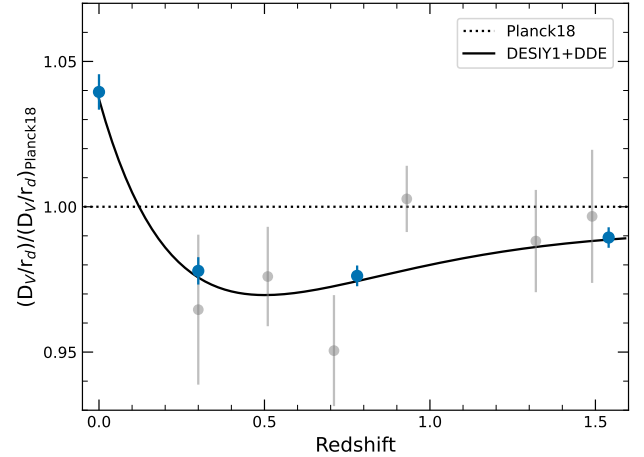


FIG. 6. Acoustic-scale distance measurements relative to the prediction from the Planck18 model. The gray symbols with  $1\sigma$  error bars represent the isotropic BAO measurements,  $D_V(z)/r_d$ , from DESIY1 [1], shown in order of increasing redshift. The curve shows the model prediction from the DESIY1+DDE cosmology, which closely matches the BAO distance measurements (blue symbols) obtained from the halo samples in our DESIY1+DDE simulation, as listed in Table II.

tion results, while the gray symbols correspond to the acoustic-scale distance measurements obtained from the DESIY1 observational data [1]. The solid curve shows the model predictions for the DESIY1+DDE cosmology, with the corresponding values at the simulation redshifts listed in the first column of Table II. We find that both the simulation results and the model predictions for the DESIY1+DDE cosmology are in excellent agreement with the observational data. The DDE model predicts a different effective distance scale than  $\Lambda\text{CDM}$ , reflecting modifications to the late-time cosmic expansion rate. At these redshifts, the Planck18 model places the BAO peak at a slightly larger separation compared to the DESIY1+DDE model, due to its larger sound horizon. This implies that the fiducial  $\Lambda\text{CDM}$  cosmology predicts a larger volume-averaged distance,  $D_V(z)$ , at these epochs.

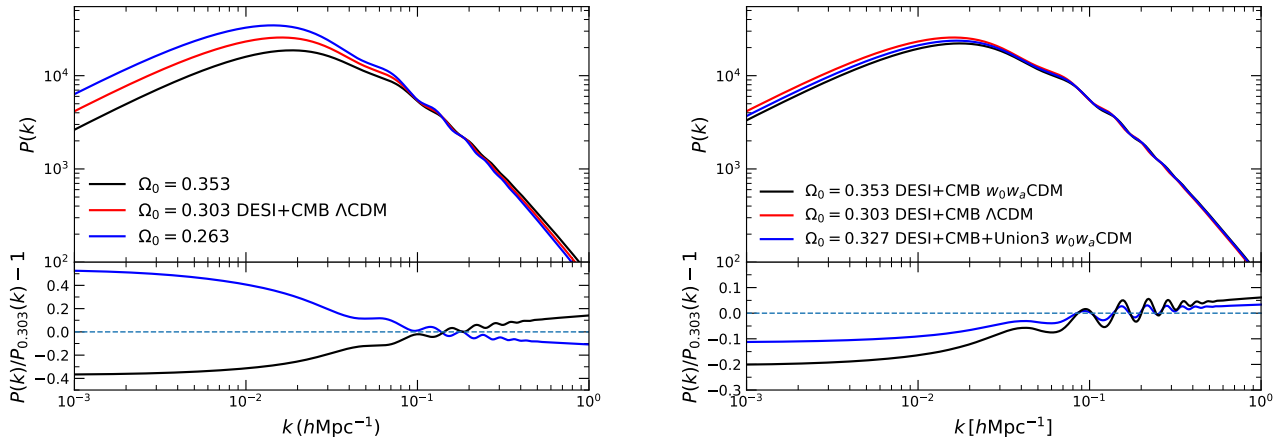


FIG. 7. Power spectra of dark matter fluctuations for different cosmological models. All power spectra are normalized to have  $\sigma_8 = 0.810$ . The left panel shows models with the same Hubble constant but varying  $\Omega_0$ . The model with  $\Omega_0 = 0.303$  corresponds to the DESIY3+CMB+ $\Lambda$ CDM model [2], shown as the red curve. For illustrative purposes, two additional models are included by artificially changing  $\Omega_0$  by about 15%. Note the substantial difference at both small and large scales. The right panel presents models chosen to have the same value of  $\Omega_0 h^2 \approx 0.143$ , favored by DESIY3 observations. When this parameter is held fixed, the differences between the models are significantly reduced, although small variations remain.

## V. DISCUSSION

How does time-varying dark energy affects the clustering of dark matter and halos? As we shown above (see, for example, Figures 2 and 4), simply modifying the dark energy equation of state – while keeping other cosmological parameters fixed – has only a modest impact on clustering. However, once the dark energy is allowed to vary, analysis of DESIY3 observational data yields significantly different best-fit cosmological parameters and power spectra, which in turn lead to noticeable changes in clustering and halo abundances. At first glance, this suggests that a wide range of configurations is now possible – at least at the 10-20 percent level. For instance, DESIY3 results [2] for the DESI+CMB+ $\Lambda$ CDM model favor  $\Omega_0 = 0.303$  and  $h = 0.682$ . In contrast, allowing for a time-varying dark energy equation of state (DESI+CMB+ $w_0 w_a$ CDM) gives best-fit values of  $\Omega_0 = 0.353$  and  $h = 0.636$  – a significant shift.

The freedom in parameter space is actually more limited than it may initially appear when one considers the power spectrum of fluctuations. The overall shape of  $P(k)$  is tightly constrained by the product  $\Omega_0 h^2$ , which determines the epoch of matter-radiation equality and, consequently, the location of the turnover scale  $k_{\text{max}}$  in the power spectrum. Shifting this position leads to significant changes in the shape and amplitude of the power spectrum across a wide range of scales.

The left panel of Figure 7 illustrates how the power spectrum  $P(k)$  responds to changes in  $\Omega_0 h^2$ . In this example, we fix the Hubble constant ( $h = 0.682$ ) and keep all other parameters constant ( $\sigma_8 = 0.810$ ,  $n_s = 0.96$ ,  $\Omega_b h^2 = 0.02218$ ), while varying  $\Omega_0$ . Set-

ting  $\Omega_0 = 0.303$  reproduces the power spectrum of DESI+CMB+ $\Lambda$ CDM model [1], shown as the red curve. For illustrative purposes, we also include two additional models where  $\Omega_0$  is artificially increased or decreased by about 15%. The resulting power spectra are shown as the blue curve (with the same  $\Omega_0 = 0.353$  as in DESI+CMB+ $w_0 w_a$ CDM) and the black curve (with  $\Omega_0 = 0.263$ ).

Note how position of the maximum,  $k_{\text{max}}$ , shifts toward larger wavenumbers with increasing  $\Omega_0$ . This shift is caused by the earlier matter-radiation equality epoch in models with higher  $\Omega_0$ , which pushes all relevant physical scales to smaller sizes and thus higher  $k$  values. We impose the condition that all spectra have the same value of  $\sigma_8$ . Since the integral defining  $\sigma_8$  is dominated by contributions around  $k \sim 0.1 h \text{ Mpc}^{-1}$ , the power spectra are nearly the same in the range  $k = 0.1 - 0.3 h \text{ Mpc}^{-1}$ . The left panel of Figure 7 clearly demonstrates that a  $\sim 15\%$  change in  $\Omega_0 h^2$  leads to substantial modifications of the power spectrum: about 40% at  $k = 0.01 h \text{ Mpc}^{-1}$  and  $\sim 15\%$  at  $k = 1 h \text{ Mpc}^{-1}$ .

Observations favor a different scenario: while individual estimates of  $\Omega_0$  and  $h$  can vary as much as 10 – 20%, depending on the observational constraints used, their product  $\Omega_0 h^2$  remains nearly constant. Figure 8 shows estimates of  $\Omega_0 h^2$  from a dozen of different data combinations analyzed in the DESIY3 paper [2]. Some estimates are based on the standard  $\Lambda$ CDM model, while others assume DDE models. Remarkably, all estimates fall within a narrow  $\sim 1 - 2\%$  range around  $\Omega_0 h^2 = 0.143$ . Not surprisingly, this is the value adopted in all our  $N$ -body simulations.

The right panel of Figure 7 illustrates what happens to



## VI. SUMMARY

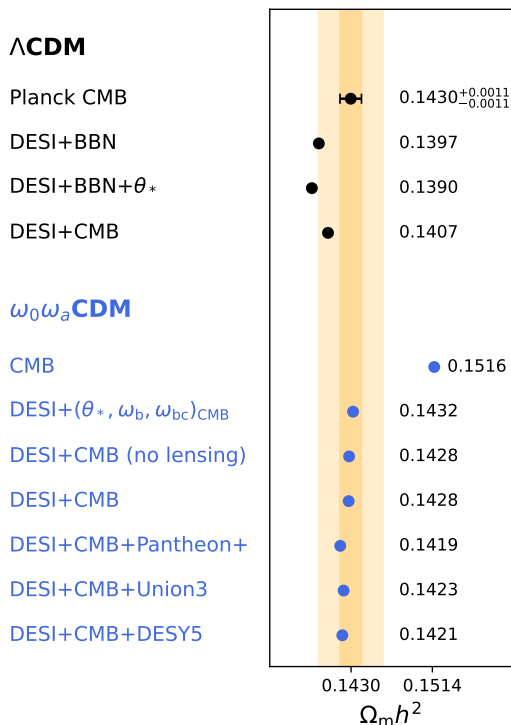


FIG. 8. Estimates of  $\Omega_0 h^2$  from various datasets and cosmological models, as analyzed in the DESIY3 paper DESI Collaboration et al. [2]. Some estimates are based on the standard  $\Lambda$ CDM model, while others assume a  $w_0 w_a$ CDM model. Most values lie within a narrow  $\sim 1-2\%$  range around  $\Omega_0 h^2 = 0.143$ . The vertical shaded bends indicate the  $1\sigma$  and  $3\sigma$  errors derived from Planck CMB data. The only significant outlier corresponds to CMB constraint under the DDE model, which is associated with large intrinsic uncertainties.

power spectrum when  $\Omega_0 h^2$  is held fixed. We show results for three models with nearly identical  $\Omega_0 h^2 = 0.143$ , but varying matter density: from  $\Omega_0 = 0.303$  for the plain  $\Lambda$ CDM model (DESI+CDM+ $\Lambda$ CDM) to  $\Omega_0 = 0.353$  for DESI+CMB+Union3+ $w_0 w_a$ CDM model (see [1]). When  $\Omega_0 h^2$  is fixed, the differences between the power spectra become much smaller, although some differences still remain.

Importantly, DDE models do not significantly modify the inferred value of  $\Omega_0 h^2$  compared to  $\Lambda$ CDM. Even across different DDE models – depending on whether supernova data are included or not – the estimate of  $\Omega_0 h^2$  remains robust. This indicates that observational data strongly constrain the shape of the power spectrum, while the impact of dynamical dark energy appears to be secondary.

If observations such as those from DESI confirm that a simple dark energy model with a constant equation of state  $w$  is insufficient, astronomers will need to consider alternative frameworks. To investigate the impact of a time-dependent  $w$ , we perform three large cosmological  $N$ -body simulations based on the Chevallier-Polarski-Linder (CPL) parametrization [5, 6]. The first simulation, labeled Planck18, serves as a benchmark and follows the the plain  $\Lambda$ CDM model. The second simulation, Planck18+DDE, adopts the CPL model for the dark energy equation of state, while keeping all other parameters identical to those in Planck18. Comparing these two simulations allows us to isolate the effects of a time-varying equation of state. The third simulation, DESIY1+DDE, includes both a dynamical dark energy component and cosmological parameters constrained by DESIY1 data. A comparison between DESIY1+DDE and Planck18+DDE highlights the impact of varying the remaining cosmological parameters while holding the dark energy parametrization fixed. The main findings of our study are summarized below.

- We find that for all statistics we studied – the matter power spectrum, halo mass function, and halo clustering – the impact of the DDE alone is smaller than the effect of the differences in cosmological parameters between Planck18 and DESIY1.
- Current observations favor cosmological models with nearly the same value of the product  $\Omega_0 h^2$  [2]. Estimates based on both plain  $\Lambda$ CDM and DDE models consistently fall within a narrow  $\sim 1-2\%$  range around  $\Omega_0 h^2 = 0.143$ .
- The non-linear matter power spectra show that the Planck18+DDE model exhibits a small ( $\sim 2\%$ ) enhancement over Planck18 at intermediate scales  $0.1 < k < 10 h \text{ Mpc}^{-1}$  for  $z > 1$ , driven by differences in the linear growth factor. By  $z = 0.3$ , this difference in the power spectra nearly vanishes. In contrast, DESIY1+DDE exhibits significantly larger deviations relative to the Planck18 model. In the linear regime, the power spectrum shows up to 5% excess at small scales  $k \gtrsim 0.2 h \text{ Mpc}^{-1}$  and a 15% suppression at large scales  $k < 0.1 h \text{ Mpc}^{-1}$ . These differences become smaller in the nonlinear regime but remain substantial, reaching 4-6% at  $k \gtrsim 1 h \text{ Mpc}^{-1}$ .
- The halo mass function reflects these trends, with DESIY1+DDE predicting up to 70% more massive halos at  $z = 2$ , and sustaining a 40% excess at  $z = 0.3$ .
- Clustering analysis reveals a 3.71% shift of the BAO peak towards smaller scales in the DESIY1+DDE model, resulting from the reduced

sound horizon scale compared to Planck18. Measurements of the  $\alpha$  dilation parameter, using halo samples with DESI-like tracer number densities across redshifts  $0 < z < 1.5$ , yield values consistent with the DESIY1+DDE-to-Planck18 sound horizon ratio. After accounting for cosmology-dependent distances, the simulation-based observational dilation parameter closely matches DESI Y1 observations.

## ACKNOWLEDGMENTS

This work has been supported by IAAR Research Support Program in Chiba University Japan,

MEXT/JSPS KAKENHI (Grant Number JP19KK0344 and JP23H04002), MEXT as “Program for Promoting Researches on the Supercomputer Fugaku” (JPMXP1020230406 and JPMXP1020230407), and JICFuS. Numerical computations were carried out on the supercomputer Fugaku provided by the RIKEN Center for Computational Science (Project ID: hp240184). FP and AK acknowledge support from the Spanish MICINN PID2021-126086NB-I00 funding grant. The data release used the the Skies & Universes database, hosted at the skun@IAA computer managed by the IAA-CSIC in Spain, through MICINN EU-Feder grant EQC2018-004366-P.

- 
- [1] A. G. Adame, J. Aguilar, S. Ahlen, S. Alam, D. M. Alexander, M. Alvarez, O. Alves, A. Anand, U. Andrade, E. Armengaud, et al., *J. Cosmology Astropart. Phys* **2025**, 021 (2025), 2404.03002.
  - [2] DESI Collaboration, M. A. Karim, J. Aguilar, S. Ahlen, S. Alam, L. Allen, C. Allende Prieto, O. Alves, A. Anand, U. Andrade, et al., *arXiv e-prints arXiv:2503.14738* (2025), 2503.14738.
  - [3] Planck Collaboration, N. Aghanim, Y. Akrami, M. Ashdown, J. Aumont, C. Baccigalupi, M. Ballardini, A. J. Banday, R. B. Barreiro, N. Bartolo, et al., *Astron. Astrophys.* **641**, A6 (2020), 1807.06209.
  - [4] B. Ratra and P. J. E. Peebles, *Phys. Rev. D* **37**, 3406 (1988), URL <https://link.aps.org/doi/10.1103/PhysRevD.37.3406>.
  - [5] M. Chevallier and D. Polarski, *International Journal of Modern Physics D* **10**, 213 (2001), gr-qc/0009008.
  - [6] E. V. Linder, *Phys. Rev. Lett.* **90**, 091301 (2003), *astro-ph/0208512*.
  - [7] H. K. Jassal, J. S. Bagla, and T. Padmanabhan, *Phys. Rev. D* **72**, 103503 (2005), URL <https://link.aps.org/doi/10.1103/PhysRevD.72.103503>.
  - [8] E. M. Barboza and J. S. Alcaniz, *Physics Letters B* **666**, 415 (2008), 0805.1713.
  - [9] A. Klypin, A. V. Macciò, R. Mainini, and S. A. Bonometto, *Astrophys. J.* **599**, 31 (2003), *astro-ph/0303304*.
  - [10] L. Casarini, A. V. Macciò, and S. A. Bonometto, *J. Cosmology Astropart. Phys* **2009**, 014 (2009), 0810.0190.
  - [11] J. M. Alimi, A. Füzfa, V. Boucher, Y. Rasera, J. Courtin, and P. S. Corasaniti, *Mon. Not. R. Astron. Soc.* **401**, 775 (2010), 0903.5490.
  - [12] S. Pfeifer, I. G. McCarthy, S. G. Stafford, S. T. Brown, A. S. Font, J. Kwan, J. Salcido, and J. Schaye, *Mon. Not. R. Astron. Soc.* **498**, 1576 (2020), 2004.07670.
  - [13] G. D. Beltz-Mohrmann, A. Pope, A. Alarcon, M. Buehlmann, N. Frontiere, K. Hearin, Andrew P. and Heitmann, S. Ortega-Martinez, A. Pearl, E. Rangel, T. Uram, et al., *arXiv e-prints arXiv:2503.05947* (2025), 2503.05947.
  - [14] D. Potter, J. Stadel, and R. Teyssier, *Computational Astrophysics and Cosmology* **4**, 2 (2017), 1609.08621.
  - [15] K. Heitmann, H. Finkel, A. Pope, V. Morozov, N. Frontiere, S. Habib, E. Rangel, T. Uram, D. Korytov, H. Child, et al., *Astrophys. J. Supp.* **245**, 16 (2019), 1904.11970.
  - [16] T. Ishiyama, F. Prada, A. A. Klypin, M. Sinha, R. B. Metcalf, E. Jullo, B. Altieri, S. A. Cora, D. Croton, S. de la Torre, et al., *Mon. Not. R. Astron. Soc.* **506**, 4210 (2021), 2007.14720.
  - [17] Q. Wang, L. Gao, and C. Meng, *Mon. Not. R. Astron. Soc.* **517**, 6004 (2022), 2206.06313.
  - [18] N. Frontiere, K. Heitmann, E. Rangel, P. Larsen, A. Pope, I. Sultan, T. Uram, S. Habib, S. Rizzi, J. Insley, et al., *Astrophys. J. Supp.* **259**, 15 (2022), 2109.01956.
  - [19] M. Michaux, O. Hahn, C. Rampf, and R. E. Angulo, *Mon. Not. Roy. Astron. Soc.* **500**, 663 (2020), 2008.09588.
  - [20] O. Hahn, C. Rampf, and C. Uhlemann, *Mon. Not. Roy. Astron. Soc.* **503**, 426 (2021), 2008.09124.
  - [21] A. Lewis, A. Challinor, and A. Lasenby, *Astrophys. J.* **538**, 473 (2000), *astro-ph/9911177*.
  - [22] T. Ishiyama, T. Fukushige, and J. Makino, *Publ. of the Astron. Society of Japan* **61**, 1319 (2009), 0910.0121.
  - [23] T. Ishiyama, K. Nitadori, and J. Makino, in *Proc. Int. Conf. High Performance Computing, Networking, Storage and Analysis, SC'12 (Los Alamitos, CA: IEEE Computer Society Press)*, 5:, (*arXiv:1211.4406*) (2012), ISBN 978-1-4673-0804-5, URL <http://dl.acm.org/citation.cfm?id=2388996.2389003>.
  - [24] T. Ishiyama, K. Yoshikawa, and A. Tanikawa, in *International Conference on High Performance Computing in Asia-Pacific Region (Association for Computing Machinery, New York, NY, USA, 2022)*, HPCAsia2022, p. 10–17, ISBN 9781450384988, URL <https://doi.org/10.1145/3492805.3492816>.
  - [25] K. Nitadori, J. Makino, and P. Hut, *New Astronomy* **12**, 169 (2006), *arXiv:astro-ph/0511062*.
  - [26] A. Tanikawa, K. Yoshikawa, T. Okamoto, and K. Nitadori, *New Astronomy* **17**, 82 (2012), 1104.2700.
  - [27] A. Tanikawa, K. Yoshikawa, K. Nitadori, and T. Okamoto, *New Astronomy* **19**, 74 (2013), 1203.4037.
  - [28] K. Yoshikawa and A. Tanikawa, *Research Notes of the American Astronomical Society* **2**, 231 (2018).
  - [29] T. Tokue, T. Ishiyama, K. Osato, S. Tanaka, and P. Behroozi, *arXiv e-prints arXiv:2412.18629* (2024),

- 2412.18629.
- [30] P. S. Behroozi, R. H. Wechsler, and H.-Y. Wu, *Astrophys. J.* **762**, 109 (2013), 1110.4372.
  - [31] M. Sinha and L. Garrison, in *Software Challenges to Exascale Computing*, edited by A. Majumdar and R. Arora (Springer Singapore, Singapore, 2019), pp. 3–20, ISBN 978-981-13-7729-7, URL [https://doi.org/10.1007/978-981-13-7729-7\\_1](https://doi.org/10.1007/978-981-13-7729-7_1).
  - [32] M. Sinha and L. H. Garrison, *Mon. Not. R. Astron. Soc.* **491**, 3022 (2020).
  - [33] S. D. Landy and A. S. Szalay, *Astrophys. J.* **412**, 64 (1993).
  - [34] D. J. Eisenstein and W. Hu, *Astrophys. J.* **496**, 605 (1998), [astro-ph/9709112](https://arxiv.org/abs/astro-ph/9709112).
  - [35] A. Klypin, V. Poulin, F. Prada, J. Primack, M. Kamionkowski, V. Avila-Reese, A. Rodriguez-Puebla, P. Behroozi, D. Hellinger, and T. L. Smith, *Mon. Not. R. Astron. Soc.* **504**, 769 (2021), 2006.14910.
  - [36] F. Prada, C. G. Scóccola, C.-H. Chuang, G. Yepes, A. A. Klypin, F.-S. Kitaura, S. Gottlöber, and C. Zhao, *Mon. Not. R. Astron. Soc.* **458**, 613 (2016), 1410.4684.
  - [37] D. J. Eisenstein, I. Zehavi, D. W. Hogg, R. Scoccimarro, M. R. Blanton, R. C. Nichol, R. Scranton, H.-J. Seo, M. Tegmark, Z. Zheng, et al., *Astrophys. J.* **633**, 560 (2005), [astro-ph/0501171](https://arxiv.org/abs/astro-ph/0501171).